ELSEVIER

Chemical Geology 141 (1997) 19–31

CHEMICAL GEOLOGY
INCLUDING
ISOTOPE GEOSCIENCE

The incorporation of Pb into zircon

E.B. Watson [a,*], D.J. Cherniak [a], J.M. Hanchar [a,b], T.M. Harrison [c], D.A. Wark [a]

[a] *Earth and Environmental Sciences Department, Rensselaer Polytechnic Institute, Troy, NY 12180, USA*
[b] *Environmental Research Division, Argonne National Laboratory, Argonne, IL 60439, USA*
[c] *Earth and Space Sciences Department, University of California, Los Angeles, CA 90024, USA*

Received 18 October 1996; accepted 29 January 1997

Abstract

The incorporation of Pb into zircons grown from Pb-rich solutions was evaluated using three different approaches: (1) high-temperature growth of large crystals from Pb–silicate melts; (2) hydrothermal overplating of thin epitaxial layers on substrates of natural zircon; and (3) growth of small, homogeneously nucleated crystals from aqueous fluids. The melt-grown zircons (50–400 μm) were crystallized from $PbO–SiO_2–ZrO_2$ ($\pm P_2O_5$) liquid at atmospheric pressure by cooling from 1430° to 1350°C. In the P_2O_5-free system, despite 66 wt% PbO in the melt, these zircons contain < 1 ppm Pb, yielding an apparent crystal/melt partition coefficient (D_{Pb}) for Pb^{2+} of 7×10^{-7}. Addition of ~ 5 wt% P_2O_5 to the melt results in uptake not only of P (~ 3400 ppm) in the zircons but also Pb (~ 1500 ppm), increasing the apparent D_{Pb} to about 10^{-3}. Hydrothermal overplating of $ZrSiO_4$ was carried out at 1.5 GPa in a piston-cylinder apparatus by slow cooling from 500°C or 550°C to 140°C of polished slabs of natural zircon immersed in zircon-saturated aqueous solutions containing either PbO_2 or $PbO + P_2O_5$. In both cases, the resulting epitaxial layers of $ZrSiO_4$ (~ 60 nm thick) contain > 3 atom% Pb, with apparent zircon/fluid partition coefficients of 4.2 and 2.6, respectively, for Pb^{4+} and Pb^{2+}. In contrast to the case of melt-grown zircons, available P is excluded from the aqueous epitaxial zircon, suggesting that charge balance is accomplished by H^+ instead. Small (2–5 μm) zircons grown by cooling aqueous solutions ($PbO + SiO_2 + ZrO_2 \pm P_2O_5$) from 800°C or 900°C contain ~ 0.25–0.5 atom% Pb (~ 2–4 wt% PbO), yielding apparent D_{Pb} values of ~ 0.2–0.3. Available P^{5+} is incorporated in a 2:1 ratio with Pb^{2+}, suggesting a specific charge-balance mechanism: $[2P^{5+} + Pb^{2+}] = [2Si^{4+} + Zr^{4+}]$. However, Pb enters the zircon even when P is unavailable, so H^+ may again play a charge-balancing role.

Because of the rapid, polythermal modes of zircon growth and the high Pb content of the experimental systems, the apparent partition coefficients should not be viewed as equilibrium values, but as qualitative indicators of Pb compatibility under various growth circumstances. The overall results are consistent with the low but variable levels of non-radiogenic (common) Pb in natural zircons. The increased compatibility of Pb in fluid-grown, low-temperature zircons suggests a possible fingerprint for zircons from hydrothermal and wet-metamorphic rocks, i.e., high concentrations of common Pb.

Keywords: zircon; lead; isotopes; crystal growth; crystal chemistry

* Corresponding author. FAX: (518) 276 8627; E-mail: watsoe@rpi.edu.

PII S0009-2541(97)00054-5

1. Introduction

Because of the key role of zircon in U–Th–Pb dating of crustal events, it is important to understand the equilibrium and kinetic behavior of both the parent (U, Th) and daughter (Pb) elements in the zircon lattice. Natural zircons concentrate U and Th during growth and tend to reject Pb, so most Pb in zircons is produced in situ from decay. However, non-radiogenic Pb (~ 2 ppb to 80 ppm; see Section 5.2) is present even in zircons apparently unaffected by contamination or metamictization, so the question arises as to what circumstances favor the incorporation of Pb into the zircon lattice.

In our ongoing experimental study of Pb diffusion in zircon, we have tried several approaches to the synthesis of Hf-free zircon containing sufficient Pb to measure using analytical techniques suitable for the depth profiling of short diffusion gradients [i.e., Rutherford backscattering spectroscopy (RBS) or ion microprobe analysis]. To date we have succeeded in growing crystals up to 500 μm in length, and also in doping $ZrSiO_4$ with significant amounts of Pb, but unfortunately (for our purposes) we have not yet achieved both goals at the same time. Nevertheless, in the process of trying, we have made some discoveries about the compatibility of Pb in zircon that may be of interest to isotope geochemists.

2. Oxidation state of Pb in the Earth's crust

An important question in assessing the compatibility of Pb in zircon concerns its oxidation state in natural environments. Of the three possibilities — Pb^0, Pb^{2+} and Pb^{4+} — only the last has an ionic radius and charge that is conducive to substitution for Zr^{4+} in the zircon lattice (the radii of Pb^{4+} and Zr^{4+} are 0.94 Å and 0.84 Å, respectively, in 8-fold coordination; for comparison, that of U^{4+} is 1.00 Å and Th^{4+} is 1.05 Å, Shannon, 1976). Fig. 1 shows the stable phases in the Pb–O system as a function of temperature and oxygen fugacity, with some familiar geologic oxygen buffers for reference. The diagram reveals that the stable form of Pb at the igneous or metamorphic conditions appropriate to zircon growth is either Pb^0 or Pb^{2+} (the latter is stable only in relatively 'oxidized' rocks), so it is not

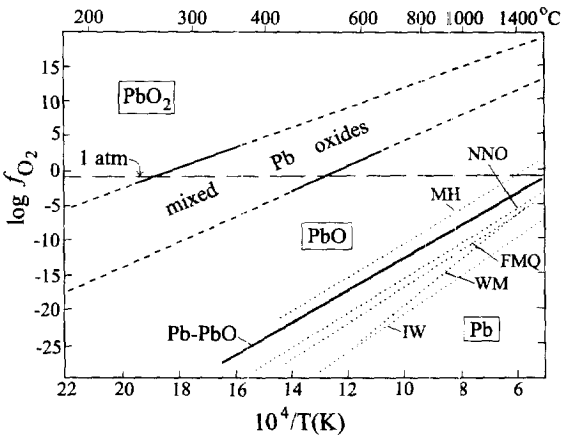

Fig. 1. Stable phases in the system Pb–O as a function of oxygen fugacity (f_{O_2}) and reciprocal absolute temperature. The heavy lines define the stability fields of various Pb–O phases, including PbO_2 (upper left), PbO and Pb metal (lower right); the lines are dashed where they lie well beyond the ranges of T and f_{O_2} investigated by experiment. The Pb–O data are from White and Roy (1964) and Otto (1966). The light, dotted lines represent several familiar 'geologic' f_{O_2} buffer curves; NNO = nickel/nickel oxide; MH = magnetite/hematite; FMQ = fayalite/magnetite/quartz; WM = wüstite/magnetite; IW = iron/wüstite. The stippled field delineates the probable range in f_{O_2} values of crustal rocks; the horizontal dashed line is atmospheric f_{O_2}. See text for discussion.

surprising that Pb exhibits broadly incompatible behavior toward zircon. On the other hand, it cannot be assumed that Pb^{2+} is totally excluded during growth, either: zircon can accommodate some altervalent substitutions to quite high concentrations even without charge-balancing cations (e.g., 1.2 wt% Dy^{3+} for Zr^{4+}; Hanchar, 1996).

In referring to Fig. 1, it is important to bear in mind that it applies strictly only to the pure Pb–O system, and that the stability fields of the various oxidation states of Pb may be significantly different in complex geologic systems. For example, Pb^{2+} could be present in a melt or metamorphic fluid at conditions more reducing than those implied by Fig. 1 — stabilized, perhaps, by formation of complexes with Cl (see, e.g., Helgeson, 1964). In any case, the relatively high concentrations of Pb in feldspars (Smith, 1983; Faure, 1986), in which Pb is almost certainly divalent, indicate that Pb^{2+} is much more abundant in crustal rocks (relative to Pb) than one would infer from Fig. 1.

3. Zircon syntheses

3.1. Crystals grown from $PbO–SiO_2–ZrO_2$ melts

The original objective in synthesizing zircons was to dope the crystals with Pb at a level of 100–1000 ppm. The initial strategy was one of 'brute force'; rather than attempt to maintain the 4+ oxidation state of Pb to the high temperatures needed for growth of a refractory phase like zircon (which appears difficult in the light of Fig. 1), we opted for growth from a very PbO-rich silicate melt. With PbO as a major component of the system, a low Pb^{2+} partition coefficient (even one as low as 0.001) would still yield sufficient Pb in the zircon for use in diffusion studies. Our base flux was a composition near the high-silica eutectic in the $PbO–SiO_2$ system at 70 wt% PbO, 30 wt% SiO_2. Because quartz is the liquidus phase of this composition (at ~850°C), we anticipated saturation in zircon (as opposed to baddeleyite) as ZrO_2 was added to the system. In a series of preliminary quenching experiments, the solubility of ZrO_2 in the base flux at 1450°C was determined as 5.7 wt%, at which point the melt reaches saturation in zircon (see 'batch 3' in Table 1 for melt composition).

Approximately 300 mg of the 3-component mixture described above was loaded into an 8-mm diameter Pt tube that was subsequently welded shut to prevent Pb volatilization at run conditions (see Fig. 2A). The tube was suspended in air (where PbO is stable at 520° < 1800°C; see Fig. 1) in a vertical-tube furnace equipped with a programmable temperature controller. Several exploratory time–temperature paths were attempted before arriving at the one shown in Fig. 2B, which produces a quenched charge consisting of glass in addition to 1.5–2% well-formed zircon crystals ranging between ~50 and 400 μm in length ('batch 3' zircons; see Table 2). The zircons were readily separated from the surrounding glass by crushing the charge and dissolving away the Pb–silicate glass in dilute HF.

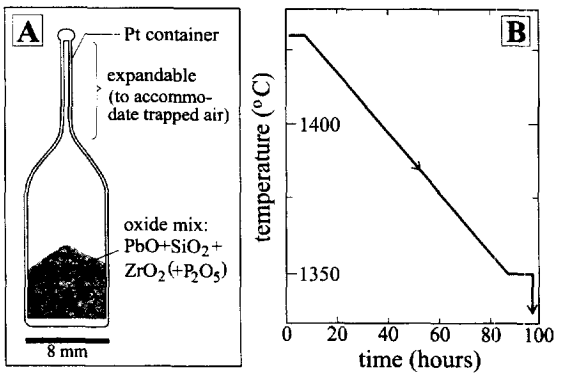

Fig. 2. (A) Platinum container used for zircon growth at atmospheric pressure from $PbO–SiO_2–ZrO_2$ ($\pm P_2O_5$) melts. (B) Time–temperature paths for batch 3 and batch 5 synthesis runs. See text and Table 1.

3.2. Crystals grown from $PbO–SiO_2–ZrO_2–P_2O_5$ melts

The zircons grown from the simple $PbO–SiO_2–ZrO_2$ melt incorporated remarkably little Pb (see Section 4), so other strategies were adopted. In-

Table 1
Summary of starting compositions expressed as wt% oxides

	Batch 3 [a]	Batch 5 [a]	PBZ6	PBZ7	PBZ8	PBZ9
SiO_2	28.3	27.0	4.3 [c]	3.2 [c]	4.3 [c]	12.8 [c]
ZrO_2	5.7	5.4	3.5 [d]	2.6 [d]	3.5 [d]	11.5 [d]
PbO_2	–	–	5.2	–	–	–
PbO	66.0	62.8	–	7.5	10.3	12.3
P_2O_5	–	4.8 [b]	–	1.5 [b]	2.0	–
H_2O	–	–	87.0	85.2	79.9	63.4

[a] Pre-fused prior to zircon synthesis.
[b] From $(NH_4)_2HPO_4$; devolatilized at ~500°C before use.
[c] Added as SiO_2 glass.
[d] From $Zr(SO_4)_2 \cdot 4H_2O$; devolatilized before use.

Table 2
Synthesis conditions and analyses of zircons grown from Pb–silicate melt

	Batch 3	Batch 5
$T–t$	1430°C → 1350°C @ 1°/h	1430°C → 1350°C @ 1°/h
P (MPa)	0.1	0.1
SiO_2 (wt%)	32.8	31.3
ZrO_2 (wt%)	67.2	67.8
Pb (ppm)	0.40±0.05 [a]	1500±100
P (ppm)	n.d	3400±50
D_{Pb}	7×10^{-7}	$\sim 10^{-3}$

Compositions were determined by electron microprobe except where noted otherwise.
[a] UCLA ion microprobe analysis (see text).

trigued by T. Krogh's passing comment (pers. commun., 1995) "common Pb in natural zircons seems to be accompanied by high phosphorus contents", we added ~ 5 wt% P_2O_5 to the original PbO–SiO_2–ZrO_2 flux mixture (see 'batch 5' in Table 1). This addition had little effect on ZrO_2 solubility, and zircon remained the liquidus phase. The mix was sealed in a Pt container and subjected to a temperature–time path similar to that shown in Fig. 2. The quenched product was ~ 85% glass with dispersed crystals of Pb–silicate and numerous small, stubby zircons averaging ~ 60 μm in size ('batch 5' zircons; see Table 2). As before, the charge was gently crushed and the Pb-rich silicate material was removed from the zircons by treatment in dilute HF. The zircons in the final separate were neither as large nor as inclusion-free as those grown from the 3-component flux (batch 3). However, they contained orders of magnitude more Pb (see Section 4).

3.3. Hydrothermal overplating on a zircon substrate

3.3.1. Rationale and general description of method

Additional attempts to synthesize zircon were made under hydrothermal conditions. We hoped to capitalize on the known (albeit limited) solubility of zircon in H_2O (Ayers and Watson, 1991) and also on the possibility of using transient high O_2 pressures to inhibit reduction of Pb oxides. Conventional hydrothermal syntheses in cold-seal pressure vessels were attempted, but the efforts were plagued by rapid reduction of PbO and PbO_2 to Pb° by hydrogen influx into the noble metal containers.

We then turned to a strategy involving epitaxial growth of new zircon on a pre-existing crystal substrate, which had the potential advantage of producing a large surface area of Pb-doped $ZrSiO_4$, suitable for depth-profiling by RBS after a diffusion experiment. Cold-seal pressure vessels were abandoned in favor of the piston-cylinder apparatus in order to reach higher pressures and consequent higher zircon solubilities. The piston-cylinder has the additional advantage that, because the pressure medium surrounding the sample container is not H_2O (as in the cold-seal vessels), the reduction of Pb oxides by H_2 influx is much slower.

For use as substrates in the 'overplating' experiments, zircon wafers ~ 0.5 mm thick were cut parallel to (110) from a natural, gem-quality crystal from the Mud Tank carbonatite (see Section 4). The wafers were polished on one side to 0.05 μm grit and sawn into smaller pieces ~ 1.5–2 mm^2. The runs were made using a 0.75-inch pressure cell (NaCl + Pyrex + Al_2O_3) and a pressure-sealing sample container that is a variant on designs regularly used in the RPI laboratory (see, e.g., Watson and Lupulescu, 1993). The container consists of a thick-walled Ni sleeve that is pre-oxidized on the surface to prevent interaction with the Pt liner containing the sample (see Fig. 3). The rigidity of the Ni under cold pressurization leads to a water-tight seal between the Pt gasket and the liner at the start of an experiment.

As described below, two overplating runs were carried out, one incorporating PbO_2 in the starting material, the other PbO + P_2O_5.

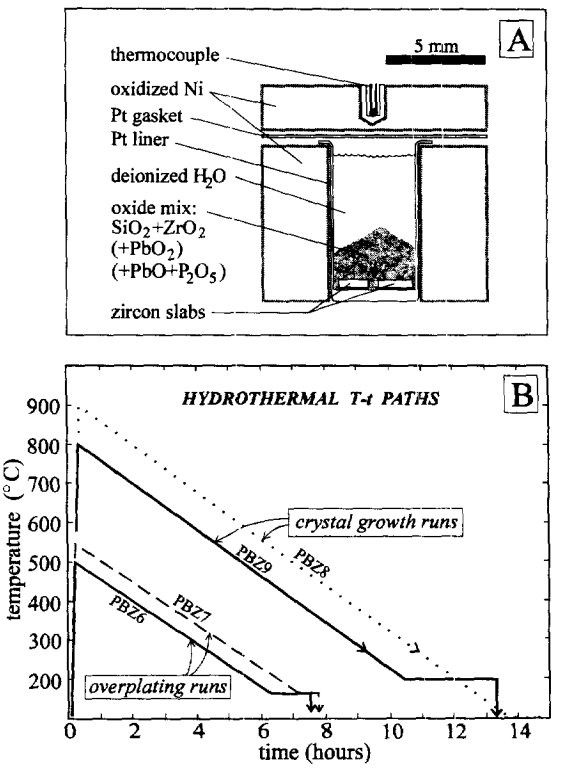

Fig. 3. (A) Platinum-lined Ni container used for experiments in the piston-cylinder apparatus. (B) Time–temperature paths for hydrothermal synthesis runs PBZ6–PBZ9. See text for details and Table 1 for starting compositions.

3.3.2. Overplating in the presence of Pb^{4+}

From the general similarity in ionic radii of Pb^{4+} and Zr^{4+}, it is reasonable to expect significant incorporation of any available Pb^{4+} into crystallizing $ZrSiO_4$. [The lattice-strain model of Blundy and Wood (1994) predicts a zircon/melt partition coefficient of ~ 100 for Pb^{4+} (Hanchar, 1996).] Accordingly, we attempted to stabilize Pb^{4+} during the growth process by keeping the temperature relatively low. Exploratory runs revealed that PbO_2 survives in the Pt-lined Ni container with H_2O for a few hours at temperatures below ~ 500°C ($P = 1.0–1.5$ GPa), as deduced qualitatively from the change in color from black (PbO_2) to yellow–orange (PbO). Significantly higher temperatures lead to rapid reduction, presumably in response to the relatively low intrinsic f_{O_2} of the pressure cell [in this case ~ nickel/nickel oxide (NNO); see Fig. 3A]. Communication between the sample and the external buffer presumably occurs by H_2 diffusion through the Pt liner (nominally dry piston-cylinder assemblies are known to contain significant moisture, e.g., Fine and Stolper, 1985).

Four substrate slabs were placed, polished side up, at the bottom of the Ni–Pt container as shown in Fig. 3A. A fine powder of $SiO_2 + ZrO_2 + PbO_2$ (PBZ6 in Table 1) was loaded directly on top of the zircon slabs, and the Pt container was topped off with deionized water. The container was then placed in the piston-cylinder assembly, pressurized to 1.5 GPa, and subjected to time–temperature path shown in Fig. 3B (run no. PBZ6). Following treatment, the zircon slabs were recovered from the container and cleaned ultrasonically in alcohol and dilute HCl to remove small amounts of adhering Pb–silicate material. Optically, the samples appeared unchanged by the hydrothermal plating process, even to the extent that the surface polish was intact.

3.3.3. Overplating from a solution containing PbO + P_2O_5

Encouraged by our earlier discovery that phosphorus markedly enhances the compatibility of Pb^{2+} in melt-grown zircon, we ran a second hydrothermal plating experiment with P_2O_5 and PbO in the aqueous growth medium. The Pt-lined container was again loaded as shown in Fig. 3A, this time with four zircon slabs plus a fine powder of $SiO_2 + ZrO_2 + PbO + P_2O_5$ (PBZ7 in Table 1). The container was subjected to the time–temperature path shown in Fig. 3B at a pressure of ~ 1.5 GPa. As before, the recovered samples were cleaned ultrasonically in alcohol and dilute HCl.

3.4. Hydrothermal synthesis by homogeneous nucleation

Because of difficulties associated with analysis of the thin zircon coatings produced in the overplating experiments, additional synthesis experiments were conducted in the piston-cylinder apparatus using a more conventional approach. Containers like those illustrated in Fig. 3A were loaded with fine powders of $SiO_2 + ZrO_2 + PbO \pm P_2O_5$ plus deionized water in the proportions shown in Table 1 (PBZ8 and PBZ9). As in the overplating experiments, rapid zircon growth was seen as essential if reduction of PbO was to be avoided, so programmed cooling at 1°/min was again used to maintain oversaturation of the solutions in zircon. Relatively high initial temperatures were also used in the hope of obtaining large crystals (800°C and 900°C for PBZ8 and PBZ9, respectively; see Fig. 3B).

Not surprisingly, these experiments resulted in crystallization of more than one phase; PBZ8 yielded Pb–phosphate + quartz + zircon; PBZ9 contained $PbSiO_3$ + quartz + zircon. The zircons were lath-shaped and very small in both cases, rarely exceeding 5 μm in length (see Fig. 4).

4. Analytical methods and results

4.1. Melt-grown zircons

The large zircons recovered from the PbO–SiO_2–ZrO_2 flux (batch 3) contain Pb concentrations below the detection limit of the electron microprobe (EMP). Subsequent determinations of the Pb content were made using the CAMECA ims 1270 ion microprobe at UCLA. Several of the synthetic crystals were mounted in an epoxy disk (2.5 cm diameter) along with fragments of Mud Tank zircon that served as a concentration standard. The Mud Tank fragments came from a ~ 10 cm^3 crystal obtained from the State Museum of Victoria (Australia); four pieces of this same crystal had been analyzed previously by

isotope dilution and found to contain 0.9 ± 0.1 ppm $^{206}Pb^*$, with a $^{206}Pb/Pb$ fraction of 85% (R.R. Parrish, pers. commun., 1996). Other gem-quality zircons from the Mud Tank carbonatite have been dated by Black and Gulson (1978) at 732 ± 5 Ma.

Ion microprobe analysis was performed using an O_2^- primary ion beam at a mass resolving power of ~6500, which is sufficient to resolve molecular interferences from the Pb isotopes. Comparison of the $^{206}Pb/^{96}Zr$ ratio of Mud Tank zircon ($2.65 \pm 0.06 \times 10^{-5}$) with that of the unknown ($6.03 \pm 0.24 \times 10^{-6}$) yields a total Pb concentration of 0.40 ± 0.05 ppm, assuming a modern common Pb isotope composition for the synthetic zircon. From the starting melt composition (Table 1), the effective zircon/melt partition coefficient (D_{Pb}) can be deduced as 7×10^{-7}.

The zircons grown from the $PbO–SiO_2–ZrO_2–P_2O_5$ flux (batch 5) were analyzed for Si, Zr, P and Pb using the JEOL 733 Superprobe (EMP) at RPI, operating at an accelerating voltage of 20 kV and a sample current of 150 nA. Collimators were used to reduce peak interferences and to maximize peak-to-background ratios. Long counting times at each spot (up to 600 s) yielded 1σ analytical uncertainties in the range of 5–10% for Pb and 1–3% for P. Matrix corrections were performed using standard ZAF techniques; element standards included synthetic zircon for Si and Zr, galena for Pb, and synthetic xenotime for P. Under these conditions, the minimum detection limits for Pb and P are 120 and 60 ppm, respectively. The P contents of the zircons grown from P-bearing melts are high and very uniform (3400 ± 50 ppm; see Table 2); P is accompanied by 1500 ± 100 ppm Pb, resulting in a Pb^{2+} partition coefficient for the P-bearing lead-silicate system (batch 5 in Table 1) of $1.1 \times 10 - 3$.

4.2. Epitaxial layers

The hydrothermally overplated zircons from the PbO_2-bearing system (run no. PBZ6) were examined first by EMP using operating conditions similar to those described above, with the beam vertically incident on the plated surface. The resulting analyses are highly reproducible from point to point and reveal remarkably high apparent Pb concentrations of 3550 ± 90 ppm (see Table 3). The stoichiometry and oxide totals are appropriate to zircon, but there is also a telltale indication that the plated layer is very thin: Hf appears in the analyses at a uniform apparent level about 20% below the known Hf abundance in the substrate Mud Tank zircon (13 100 ppm; Hanchar, 1996). Because the plating constituents contained no Hf, it was immediately clear that the electron beam was 'seeing through' the plated layer into the substrate (see Fig. 5). It was also clear that the plated layer, being thin to the incident electron beam, must have an actual Pb concentration much higher than the 3550 ppm apparent in the analyses. One of the PBZ6 plated zircons was depth-profiled by Rutherford backscattering spectrometry (RBS; see

Table 3
Experimental conditions and analyses of zircons subjected to hydrothermal overplating

	PBZ6	PBZ7
T–t	500°C → 140°C @ 60°/h	550°C → 140°C @ 60°/h
P (GPa)	1.5	1.5
Layer thickness (nm)	~54 (1 sample)	60–170 (4 samples)
SiO_2 (wt% by EMP)	32.4	32.6
ZrO_2 (wt% by EMP)	66.5	65.8
Pb (ppm by EMP)	3550 ± 90	1940 ± 130
Pb (ppm by RBS)	220 000	199 000
P (EMP, RBS)	n.d.	n.d
Hf (ppm by EMP)	10 500 ± 40	11 800 ± 45
D_{Pb} [a]	~4.2	~2.6

Electron microprobe (EMP) analyses are composite values including both the surface layer and the substrate. Analyses by Rutherford backscattering spectroscopy (RBS) represent the surface layer only. See text and Fig. 5.

[a] Estimated minimum value, assumes that all Pb in the system was initially dissolved in the aqueous fluid.

Fig. 5 and Chu et al., 1978), which confirmed the O–Si–Zr–Pb stoichiometry of the overplated layer as that of Pb-rich zircon, and established the thickness as ~ 54 nm. The Pb content averages a remarkably high ~ 22 wt% (3.7 atom%). Assuming that all Pb in the system was in solution at the initiation of epitaxial growth, the effective zircon/fluid partition coefficient is ~ 4.2. The RBS analysis provides no indication of the oxidation state of Pb, but from the starting composition (Table 1) and the qualitatively known rate of reduction in the experimental capsule (see Section 3.3.2), we infer that much of the Pb

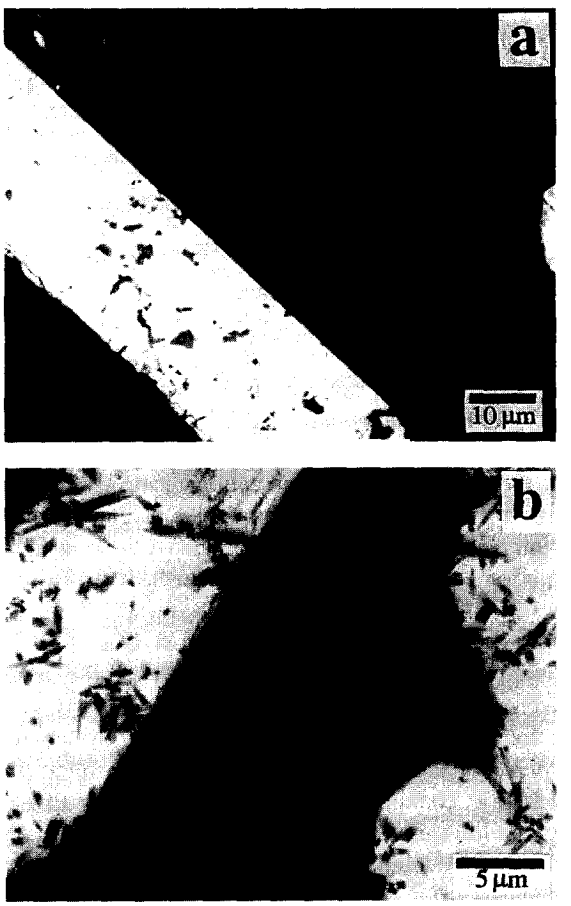

Fig. 4. Backscattered-electron images of run products from hydrothermal crystallization experiments. (a) Small zircon laths in run PBZ8 (medium gray) enclosed in large quartz grains (dark gray background). Zircons are also included in the large, white crystal, which is Pb phosphate. (b) Zircon laths (medium gray) in run PBZ9 adjacent to and included within large $PbSiO_3$ crystals (white). Black material in both photos is epoxy.

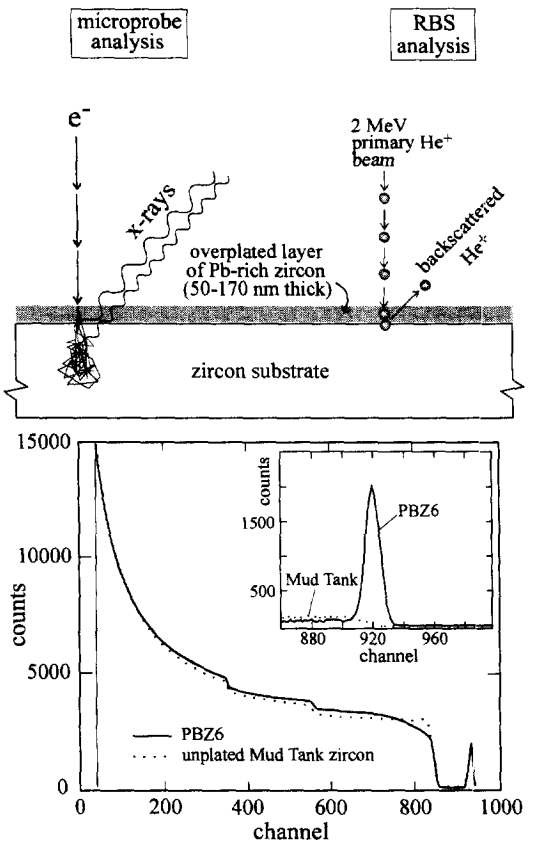

Fig. 5. *Top*: Schematic representation of the two analytical techniques used to characterize the hydrothermally overplated zircon: (1) electron microprobe analysis; and (2) Rutherford backscattering spectroscopy (RBS). In microprobe analysis, the primary electron beam interacts with the thin (Pb-rich) overplated layer and also penetrates well into the (Hf-bearing) substrate. Characteristic X-rays are generated in both layers, so the resulting analysis is a mixture of the two compositions. In RBS analysis, the primary He ion beam is backscattered from atoms in the near-surface region of the sample, providing quantitative composition vs. depth information. *Bottom*: RBS spectrum of sample PBZ6. Reduction of this spectrum reveals that the surface layer is ~ 54 nm thick and consists of stoichiometric zircon containing 22 wt% Pb. See text and Fig. 3 for details of the overplating experiments; see Cherniak and Watson (1992) for a description of RBS.

present in the overplated layers is Pb^{4+}. Hydrogen profiling by nuclear reaction analysis (NRA; see Lanford et al., 1976) revealed a high concentration of H in the layers, corresponding to a ~ 3 : 1 atomic ratio of H/Pb. The elevated H content was not unexpected in light of the results of Caruba et al. (1975, 1985), who documented up to 80% replace-

ment of SiO_4 by $(OH,F)_4$ in synthetic, hydrothermal zircons; however, without better knowledge of the oxidation state of Pb, the role of H in the Pb-bearing epitaxial zircon cannot be deduced. If all Pb is 4+, no charge compensation is needed, and $4H^+$ may simply replace Si^{4+} in the so-called hydrogrossular substitution (see Woodhead et al., 1991). If significant Pb^{2+} is present, on the other hand, some H may play a charge-compensating role (as OH^- replacing O^{2-}; see Section 5).

Like the PBZ6 samples, the zircon slabs overplated from the $PbO + P_2O_5$-bearing solution (run no. PBZ7) were analyzed by EMP and RBS, and depth-profiled using NRA for both H and P (see McIntyre et al., 1988 for the P technique). The epitaxial layers are 60–170 μm thick and contain, on average, 19.9 wt% Pb (3.3 atom%), indicating a maximum zircon/fluid partition coefficient of ~ 2.6. Surprisingly (in view of the batch 5 results), P was not detectable by EMP, RBS or NRA (Table 3; the NRA technique has a detection limit for P of ~ 800 ppm atomic), which suggests that the excess positive charge arising from replacement of Zr^{4+} by Pb^{2+} is balanced by OH^- replacing O^{2-}. This suggestion gains support from the H profiling results, which reveal variable concentrations of H up to 6% atomic, i.e., approaching H/Pb = 2.

4.3. Hydrothermal crystals

The zircons recovered from experiments PBZ8 and PBZ9 presented special analytical difficulties because of their small size (max. ~ 2 × 5 μm; see Fig. 4). Even with the electron microprobe, spatial resolution was insufficient to obtain 'clean' analyses. However, by lowering the accelerating voltage to 10 or 12 kV (for PBZ8 and PBZ9, respectively), it was possible to obtain meaningful results. Apart from a lower accelerating voltage and sample current (~ 40 nA), the analysis conditions were similar to those used for the much larger melt-grown zircons (see Section 4.1). The PBZ8 zircons were present in the run product almost exclusively as inclusions in large, euhedral quartz grains. For this reason, the microprobe analyses show a significant apparent excess of SiO_2 (Table 4) due to overlap of the X-ray excitation volume onto quartz. However, because the quartz contains no Pb or P, the measured levels of these elements in the zircons are believed to be reliable minimum estimates. Although not as high as those in the hydrothermally overplated layers, the PbO and P_2O_5 concentrations in the PBZ8 zircons are substantial: 1.8 (±0.7) and 1.3 (±0.3) wt%, respectively (Table 4). Significantly, the cationic ratio P/Pb is 2, within analytical uncertainty. The calculated minimum value for D_{Pb}, assuming that all Pb was in solution at the outset of zircon growth, is 0.17.

Table 4
Growth conditions and electron microprobe analyses of hydrothermal zircons

	PBZ8		PBZ9	
$T-t$:	900°C → 100°C @ 60°/h		800°C → 200°C @ 60°/h	
P (MPa):	1.5		1.0	
Oxide:	wt% (σ)	cat./4 ox.	wt% (σ)	cat./4 ox.
SiO_2	35.3 (3.7)	1.057	27.7 (1.24)	0.988
ZrO_2	61.2 (3.2)	0.896	57.1 (1.89)	0.995
PbO	1.8 (0.7)	0.015	3.5 (1.10)	0.034
P_2O_5	1.3 (0.3)	0.032	n.d.	
Total	99.6	2.000	88.3	2.017
D_{Pb} [a]	0.17		0.29	

The PBZ8 zircons are included in quartz, and the largest are ~ 25 μm in size (see Fig. 4a), so the analyses contain an apparent excess of SiO_2 that is probably due to analytical 'contamination'. The oxide totals of the PBZ9 zircons are low mainly because of their small size (Fig. 4b) and the fact that they are surrounded by epoxy in the microprobe mounts (a small portion of the 'deficit' may be due to replacement of Si^{4+} by H^+; see text).

[a] Estimated minimum value, assumes that all Pb in the system was initially dissolved in the aqueous fluid.

Like those in experiment PBZ8, the PBZ9 zircon laths do not exceed ~ 2 μm across (Fig. 4b), so similar analytical difficulties arose with the EMP determinations. The crystals chosen for analysis were surrounded by epoxy (in 2-D section) in the microprobe mounts, so the small crystal size resulted not in X-ray 'contamination' (as from quartz in PBZ8) but in low analysis totals, averaging ~ 88%. The Si/Zr/O stoichiometry confirms the identity of these crystals as zircon, but they contain, once again, quite high concentrations of Pb, corresponding to ~ 3% replacement of Zr atoms by Pb and a minimum zircon/fluid partition coefficient of 0.29 (Table 4).

The possibility was considered that the high apparent Pb content in the PBZ9 zircons is due to secondary fluorescence from nearby $PbSiO_3$ (see

Fig. 4b). A minor secondary fluorescence contribution to the zircon analyses cannot be ruled out, but the following two observations indicate that the high Pb levels are real: (1) there is no correlation between apparent Pb concentration and distance from $PbSiO_3$; and (2) secondary fluorescence of $PbSiO_3$ would contribute not just to Pb but also to Si count rates on zircon. The PBZ9 zircon analyses are, if anything, slightly low in Si (Table 4). Lead contamination of the zircon surfaces by smearing of $PbSiO_3$ during polishing can also be ruled out. This phenomenon has been observed during Pb isotopic analysis by ion microprobe of natural zircons in rocks containing high-Pb phases such as galena and sphalerite (A. Nutman, written commun., 1997). However, no Pb X-rays are detected during electron microprobe analysis of batch 3 zircons (virtually Pb-free; see Table 2) embedded in Pb-rich glass. The electron microprobe is simply too insensitive to 'see' this kind of contamination.

5. Discussion and conclusions

5.1. Interpretation and implications of 'partition coefficients'

In some respects, the results reported here serve only to confirm what was already known, i.e., that Pb is generally incompatible in zircon. Some interesting aspects of Pb uptake in zircon have nevertheless come to light. Considering that zircon serves as host to a wide variety of minor and trace elements (~ 50 according to some sources; e.g., Speer, 1980), the degree to which Pb^{2+} is excluded from zircon during growth from a dry, P_2O_5-free melt is surprising. Partition coefficients as low as $\sim 10^{-5}$ are unusual for lithophile elements in silicate crystals (see, e.g., Jones, 1995); at 7×10^{-7}, the D_{Pb} value for the 'batch 3' zircons is extraordinarily low. A more silicic melt composition (e.g., granite) and/or a lower growth temperature might lead to a somewhat higher partition coefficient, but these effects probably would not amount to orders of magnitude. If the 'batch 3' partition coefficient of 7×10^{-7} governed Pb behavior in natural systems, we would anticipate abundances of non-radiogenic (common) Pb in crustal zircons of only ~ 0.01 ppb (given an average crustal Pb concentration of ~ 12 ppm; Taylor, 1964), which is three orders of magnitude below typically observed levels (e.g., Krogh, 1993; see Section 5.2). This inconsistency may be explained, as Krogh (pers. commun., 1995) suspected, by a connection between P and Pb in zircon. Our P-bearing silicate melt system (batch 5) yielded an apparent Pb^{2+} partition coefficient of $\sim 10^{-3}$; operating in nature, this value would lead to common Pb levels in crustal zircons within the range of those actually observed. Clearly, the batch 5 system (Table 1) bears little resemblance to a granite, so this agreement may be fortuitous, but a role for P in the uptake of common Pb in some magmatic zircons seems probable. Crustal magmas generally contain much less than the 5 wt% P_2O_5 present in our experimental system, but the chemical activity of this component is nevertheless very high in granitic melts (perhaps higher than in our experimental system), as evidenced by widespread saturation in apatite at near-liquidus temperatures.

In the melt-grown zircons, P appears to 'overplay' its probable charge-compensation role in the uptake of Pb. The coupled substitution

$$[2P^{5+} + M^{2+}] \leftrightarrow [2Si^{4+} + Zr^{4+}] \quad (1)$$

while not documented previously, can be proposed by analogy with the well-known 'xenotime-type' exchange involving P^{5+} and Y^{3+} or REE^{3+}

$$[P^{5+} + M^{3+}] \leftrightarrow [Si^{4+} + Zr^{4+}] \quad (2)$$

(Dennen and Shields, 1956; Caruba et al., 1974; Hinton and Upton, 1991). Our analyses suggest that P^{5+} does replace Si^{4+} in the batch 5 zircons (because SiO_2 is low relative to stoichiometric $ZrSiO_4$; see Tables 2–4), but the excess positive charge arising from this substitution is not fully compensated by replacement of Zr^{4+} with Pb^{2+} (this would require $P/Pb = 2$, and the observed atomic ratio is ~ 15). The overabundance of P does not rule out the exchange represented by Eq. (1), but some additional charge-balance mechanism must operate as well. The simplicity of the system rules out candidates such as halogens or even hydrogen, leaving excess oxygen as one of few remaining possibilities. There exists at least one other example of P-doped synthetic zircon in which P^{5+} is not compensated by a low-valence substitution in the Zr^{4+} site. Hanchar (1996) found

that zircons grown from Li-molybdate flux containing P_2O_5 plus a single light rare earth element take up considerably more P^{5+} than $LREE^{3+}$. The level of P in those zircons is consistently 2400–2600 ppm, irrespective of the identity of the accompanying LREE, whose concentrations range from 140 ppm in the case of La to near (atomic) parity with P in the case of Gd.

The role of P^{5+} in the uptake of Pb^{2+} during hydrothermal growth is easier to assess. The P/Pb ratio of the PBZ8 zircons is ~ 2 [as predicted by Eq. (1)], so a straightforward charge-balance mechanism seems to operate. At growth temperatures below ~ 500°C, however, available P in hydrothermal systems is apparently excluded from crystallizing zircon, as evidenced by the results of run PBZ7. Interestingly, Pb^{2+} will still enter the zircon structure even if P^{5+} is not available for charge compensation (cf. run PBZ9), in which case charge balance is probably maintained by incorporation of H^+. Two types of substitution involving H^+ are well documented in zircon:

$$[M^{3+} + H^+] \leftrightarrow [Zr^{4+}]$$

or (3)

$$[M^{3+} + OH^-] \leftrightarrow [Zr^{4+} + O^{2-}]$$

and

$$[4H^+] \leftrightarrow [Si^{4+}] \quad (4)$$

Both occur in natural, nonmetamict zircons, but the former is generally dominant (Woodhead et al., 1991). In zircons synthesized hydrothermally, the Si^{4+} replacement mechanism [Eq. (4)] is highly effective, apparently resulting in up to 80% replacement of Si^{4+} by $4H^+$ in some instances (Caruba et al., 1975, 1985). Hydrogen profiling of the overplated layers in PBZ6 and PBZ7 reveals levels of H that are more than adequate to allow entry of Pb^{2+} into the zircon lattice (without charge-compensating P^{5+}) by the substitution

$$[Pb^{2+} + 2H^+] \leftrightarrow [Zr^{4+}] \quad (5)$$

which is analogous to the well-known substitution represented by Eq. (3).

From our hydrothermal overplating experiment in the PbO_2-bearing system, it is clear that Pb^{4+} is, as anticipated, quite compatible in zircon. This knowledge is of limited value in geochemistry because natural zircons rarely if ever grow under conditions sufficiently oxidizing to stabilize Pb^{4+} (see Fig. 1). Nevertheless, confirmation of the compatible nature of Pb^{4+} is useful, because it may lead to a convenient way of doping synthetic zircon for Pb diffusion studies.

In closing this section, it is important to underscore the highly qualitative nature of the 'partitioning' results we report. In all three synthesis approaches, there are good reasons to question the attainment of equilibrium. This is especially true of the hydrothermal epitaxial-plating runs, in which the growth rate was high despite a low prevailing temperature; optimal conditions for formation of defect-ridden zircon. It is entirely possible, also, that Pb is adsorbed on some or all growth surfaces of zircon, occupying partially formed sites as an OH- or P-bearing complex. These adsorbed complexes could become trapped in the lattice as the zircon grows, a process modeled mathematically by Watson and Liang (1995) and discussed in broad geochemical terms by Watson (1996). Perhaps not coincidentally, aqueous Pb^{2+} has been shown to be selectively adsorbed on some surfaces of α-Al_2O_3 (Bargar et al., 1996). In our view, the zircons grown from the simple PbO–SiO_2–ZrO_2 melt (batch 3) probably represent the closest approach to equilibrium, because the growth temperature was high and the cooling rate relatively low. Unfortunately, the apparent D_{Pb} value of 7×10^{-7} is probably also the least relevant to any geologic situation, because the system bears little resemblance (other than having a high molar silica content) to granite, and is also extremely Pb-rich. The other syntheses, though probably far from equilibrium, may still have value as qualitative indicators of behavioral tendencies in natural systems. We would not argue strongly for an equilibrium zircon/aqueous fluid partition coefficient for Pb^{2+} that is greater than 1 (as implied by PBZ7), but it seems reasonable to expect *some* compatibility of Pb in zircon under natural hydrothermal conditions, or at least not total incompatibility.

5.2. Consistency with nature

The amount of common Pb in natural zircons is difficult to assess from perusal of the isotope dilution

literature, for three reasons. First, unless the laboratory in which the isotopic analyses are performed has a very low and consistent Pb blank, it is not clear how much of the reported common Pb is laboratory contamination and how much is intrinsic to the zircon (see, e.g., Krogh, 1993). Second, in selecting zircons for U–Pb analysis, a deliberate sampling bias is usually applied in order to maximize the likelihood of concordant results. The selection process may involve air abrasion to remove potentially discordant material from the outer part of the zircon. Any zircons (or parts thereof) that are turbid, cracked, metamict or otherwise suspect are generally bypassed in the selection procedure, so it is conceivable that high-common Pb zircons are sometimes overlooked. Lastly, it remains unclear what fraction of the measured common Pb is dissolved in the zircon structure as opposed to being contained in small fluid-, glass- or mineral inclusions. Isotope dilution analyses should probably be viewed as upper estimates.

At the Royal Ontario Museum, where the Pb blank is 2–6 picograms (pg), Krogh (1993) determined common Pb masses in air-abraded zircons of ~ 2 to 7 pg, with most values falling below 4 pg and one 'anomalous' value of 11 pg. (Because the apparent masses of common Pb in analyzed zircons include the blank levels, the abundances in the zircons are negligible. For a typical zircon ($\sim 100 \times 30$ μm) having a mass of 300 μg, 3 pg of common Pb translates into 10 ppb.) A few other high-quality U–Pb isotopic analyses reveal higher levels of common Pb. Wiedenbeck et al. (1995), for example, reported levels up to 100 ppb in a massive (238 g), 1065 Ma-old zircon from Renfrew County, Ontario (Canada) that has been proposed for use as a U–Pb isotopic standard. Much higher concentrations of common Pb (21 and 80 ppm) were found by Corfu (1987) in two zircon fractions from the Agawa migmatite terrain in the Superior Province of Canada.

Given the latitude provided by the uncertain abundance limits of common Pb in natural zircons, the results reported here are consistent with nature. It is unnecessary to invoke growth conditions sufficiently oxidizing to stabilize Pb^{4+}, because zircons grown in a P-bearing melt or an aqueous fluid incorporate significant amounts of Pb^{2+}. Since both P and H_2O are ubiquitous in crustal geologic systems, and since Pb^{2+} is a common form of Pb in nature (see Section 2), it is reasonable that some natural zircons should contain measurable amounts of non-radiogenic Pb, despite the low abundance of Pb in the systems from which they typically crystallize.

The really intriguing aspect of common Pb in natural zircons is its apparent variability. Our Pb-doping results suggest two possible explanations. First, the variation may be due in part to differences in the ambient f_{O_2} of the growth environment. Assuming that Pb° is totally excluded from the zircon lattice during growth, zircons grown under conditions where Pb is a significant or dominant form of Pb would contain little to no common Pb. This circumstance could prevail at ambient f_{O_2} values that are geologically commonplace, i.e., anywhere below ~ NNO + 3 log units (see Fig. 1 and Section 2). Alternatively, the variation in common Pb abundance in natural zircons may simply reflect the nature of the growth environment. In our three synthetic systems, one 'igneous', the others hydrothermal, Pb^{2+} enters the zircon lattice in all cases, but the concentration in the hydrothermal zircons is much higher (and perhaps inversely correlated with temperature). It seems probable that a similar difference between hydrothermal and igneous zircons exists in nature. For U–Th–Pb isotope geochemistry, this may well be the most significant implication of this study, because it could provide a means to distinguish zircons formed in very wet environments. Our results suggest that hydrothermal (and possibly 'wet' metamorphic) zircons should contain orders of magnitude more common Pb than zircons grown under relatively dry conditions. In practice, unfortunately, it may be difficult to distinguish common Pb acquired at the time of zircon growth from common Pb gained by diffusion into a metamict crystal.

5.3. Radiogenic Pb

A remaining question is whether our results have any bearing on the compatibility of radiogenic Pb in the zircon lattice. The answer clearly depends upon the valence state of the radiogenic Pb atoms: Pb^{4+} is compatible under any circumstances but is it stable or present at all in the zircon lattice? Although a given radiogenic Pb atom is produced by radioactive decay of tetravalent ions (U^{4+} or Th^{4+}), the ener-

getic nature of the decay process almost certainly precludes conservation of electrons around the nucleus as it passes through the numerous intermediate decay products (which include an inert gas). Consequently, there is no reason to expect that radiogenic Pb atoms begin their existence in the 4 + valence state, despite a tetravalent ionic parentage. Because of the generally rapid transport of electrons and vacancies in crystals (Schmalzried, 1984), newly formed Pb atoms in zircon probably assume a valence appropriate to the f_{O_2} of the host rock. Pasteris and Wanamaker (1988) demonstrated that fluid inclusions in olivine approach f_{O_2} equilibrium with the ambient atmosphere of the host crystals in a remarkably short time (a few hours) at 1075°–1400°C. The relative rates of defect diffusion in olivine and zircon are not known, but under dry conditions oxygen diffuses at similar rates in the two minerals (cf. Ryerson et al., 1989; Watson and Cherniak, 1997). Redox equilibration of radiogenic Pb with ambient conditions has been documented in uranium ores (e.g., Sunder et al., 1992, 1994, 1996), although not specifically for the case of Pb atoms in the zircon lattice. In general, it appears likely that radiogenic Pb atoms assume the same valence state as pre-existing common Pb. As Pb accumulates over time in a zircon hosted by a normal crustal rock (i.e., one containing no more than a few ppm Pb), the system diverges increasingly from partitioning equilibrium. In other words, a Pb chemical potential gradient develops, which has logically been regarded as a 'driving force' for diffusive loss of Pb from the zircon. Whether or not this loss actually occurs depends upon how rapidly Pb diffuses in the zircon lattice, which is not fully understood (but see Cherniak et al., 1991; Bogomolov, 1991). The present study suggests additional factors that might affect the tendency and effectiveness of radiogenic Pb loss from natural zircons. For example, because maintenance of local charge balance is essential in any diffusion process, Pb^{2+} cannot simply leave the zircon structure without a charge-balancing counterflux. (This would seem to be all the more necessary because Pb^{2+} only partially compensates for the charge imbalance created by decay of 4 + ions.) In hydrous environments, the charge compensation is almost certainly accomplished by protons. Interestingly, though, our results also suggest that an influx of hydrogen would actually stabilize the radiogenic Pb in the zircon, since Pb^{2+} is incorporated into growing zircon when H^+ is available for charge compensation. In other words, influx of H^+ into a zircon that is accumulating Pb may prevent the rise in chemical potential of Pb that is implicitly regarded as necessary for Pb loss. Under such circumstances, Pb loss could occur only by exchange of radiogenic Pb with common Pb (or other cations) in the host medium.

Acknowledgements

During the course of this study, the authors benefited from discussions with Al Hofmann, Tom Krogh and Desmond Moser. Kevin McKeegan and Cris Coath provided invaluable assistance with the ion probe analyses at UCLA. This research was supported by the National Science Foundation, under grant nos. EAR-9205793 and EAR-9527014 to E.B. Watson.

References

Ayers, J.C., Watson, E.B., 1991. Solubility of apatite, monazite, zircon and rutile in supercritical aqueous fluids, with implications for subduction-zone geochemistry. Philos. Trans. R. Soc. London A 335, 365–375.

Bargar, J.R., Towle, S.N., Brown, G.E., Parks, G.A., 1996. Outer-sphere lead(II) adsorbed at specific surface sites on α-alumina. Geochim. Cosmochim. Acta 60, 3541–3547.

Black, L.P., Gulson, B.L., 1978. The age of the Mud Tank carbonatite, Strangways Range, Northern Territory. B.M.R. J. Aust. Geol. Geophys. 3, 227–232.

Blundy, J., Wood, B.J., 1994. Prediction of crystal–melt partition coefficients from elastic moduli. Nature 372, 452–454.

Bogomolov, Ye.S., 1991. Migration of lead in non-metamict zircon. Earth Planet. Sci. Lett. 107, 625–633.

Caruba, R., Turco, G., Iacconi, P., Keller, P., 1974. Solution solide d'éléments de transition trivalents dans le zircon et l'oxyde de zirconium: étude par thermoluminescence artificielle. Soc. Fr. Minéral. Crist. Bull. 97, 278–283.

Caruba, R., Baumer, A., Turco, G., 1975. Nouvelles synthèses hydrothermales du zircon: substitutions isomorphiques; relation morphologie-milieu de croissance. Geochim. Cosmochim. Acta 39, 11–26.

Caruba, R., Baumer, A., Ganteaume, M., Iacconi, P., 1985. An experimental study of hydroxyl groups and water in synthetic and natural zircons: a model of the metamict state. Am. Mineral. 70, 1224–1231.

Cherniak, D.J., Watson, E.B., 1992. A study of strontium diffusion in K-feldspar, Na-K feldspar and anorthite using Rutherford backscattering spectroscopy. Earth Planet. Sci. Lett. 113, 411–425.

Cherniak, D.J., Lanford, W.A., Ryerson, F.J., 1991. Lead diffusion in apatite and zircon using ion implantation and Rutherford backscattering techniques. Geochim. Cosmochim. Acta 55, 1663–1673.

Chu, W.K., Mayer, J.W., Nicolet, M.-A., 1978. Backscattering Spectrometry. Academic Press, Orlando, FL, 384 pp.

Corfu, F., 1987. Inverse age stratification in the Archean crust of the Superior Province: Evidence for infra- and subcrustal accretion from high resolution U–Pb zircon and monazite ages. Precambrian Res. 36, 259–275.

Dennen, W.H., Shields, R., 1956. Yttria in zircon. Am. Mineral. 41, 655–657.

Faure, G., 1986. Principles of Isotope Geology, 2nd ed. Wiley, New York.

Fine, G., Stolper, E.M., 1985. The speciation of carbon dioxide in sodium aluminosilicate glasses. Contrib. Mineral. Petrol. 91, 105–121.

Hanchar, J.M., 1996. A Geochemical Investigation of Zircon. Ph.D. Thesis, Rensselaer Polytechnic Institute, Troy, New York, 210 pp.

Helgeson, H.C., 1964. Complexing and Hydrothermal Ore Deposition. Pergamon, New York.

Hinton, R.W., Upton, B.G.J., 1991. The chemistry of zircon: Variations within and between large crystals from syenite and alkali basalt xenoliths. Geochim. Cosmochim. Acta 55, 3287–3302.

Jones, J.H., 1995. Experimental trace element partitioning. In: Ahrens, T.J. (Ed.), Rock Physics and Phase Relations: A Handbook of Physical Constants. American Geophysical Union, Washington, DC.

Krogh, T.E., 1993. High-precision U–Pb ages for granulite metamorphism and deformation in the Archean Kapuskasing structural zone, Ontario: Implications for structure and development of the lower crust. Earth Planet. Sci. Lett. 119, 1–18.

Lanford, W.A., Trautvetter, H.P., Ziegler, J.F., Keller, J., 1976. New precision technique for measuring the concentration vs. depth of hydrogen in solids. Appl. Phys. Lett. 28, 566–568.

McIntyre, L.C., Leavitt, J.A., Dezfouly-Arjomandy, B., Oder, J., 1988. Depth profiling of phosphorus using the resonances in the $^{31}P(\alpha, p)^{34}S$ reaction. Nucl. Instrum. Methods B35, 446–450.

Otto, E.M., 1966. Equilibrium pressures of oxygen over oxides of lead at various temperatures. J. Electrochem. Soc. 113, 525–527.

Pasteris, J.D., Wanamaker, B.J., 1988. Laser Raman microprobe analysis of experimentally re-equilibrated fluid inclusions in olivine: Some implications for mantle fluids. Am. Mineral. 73, 1074–1088.

Ryerson, F.J., Durham, W.B., Cherniak, D.J., Lanford, W.A., 1989. Oxygen diffusion in olivine: Effect of oxygen fugacity and implications for creep. J. Geophys. Res. 94, 4105–4118.

Schmalzried, H., 1984. Solid State Reactions, 2nd ed. Springer-Verlag, New York.

Shannon, R.D., 1976. Revised effective ionic radii and systematic studies of interatomic distances in halides and chalcogenides. Acta Cryst. A32, 751–767.

Smith, J.V., 1983. Some chemical properties of feldspars. In: Ribbe, P.H. (Ed.), Feldspar Mineralogy, 2nd ed. Reviews in Mineralogy, Vol. 2, Mineralogical Society of America, Washington, DC, pp. 281–296.

Speer, J.A., 1980. Zircon. In: Ribbe, P.H. (Ed.), Orthosilicates. Reviews in Mineralogy, Vol. 5, Mineralogical Society of America, Washington, DC, pp. 67–112.

Sunder, S., Cramer, J.J., Duclos, A.M., 1992. X-ray photoelectron spectroscopic study of Cigar Lake uranium ore: A natural analog for used fuel. In: Sombret, C.G. (Ed.), Scientific Basis for Nuclear Waste Management, XV. Materials Research Society, Pittsburgh, PA, pp. 449–457.

Sunder, S., Miller, N.H., Duclos, A.M., 1994. XPS and XRD studies of samples from the natural fission reactors in the Oklo uranium deposits. In: Barkatt, A., Van Konynenburg, R.A. (Eds.), Scientific Basis for Nuclear Waste Management, XVII. Materials Research Society, Pittsburgh, PA, pp. 631–638.

Sunder, S., Cramer, J.J., Miller, N.H., 1996. Geochemistry of the Cigar Lake uranium deposit: XPS studies. Radiochim. Acta 74, 303–307.

Taylor, S.R., 1964. The abundance of chemical elements in the earth's crust a new table. Geochim. Cosmochim. Acta 28, 1273–1285.

Watson, E.B., 1996. Surface enrichment and trace-element uptake during crystal growth. Geochim. Cosmochim. Acta 60, 5013–5020.

Watson, E.B., Cherniak, D.J., 1997. Oxygen diffusion in zircon. Earth Planet. Sci. Lett. 148, 527–544.

Watson, E.B., Liang, Y., 1995. A simple model for sector zoning in slowly grown crystals: Implications for growth rate and lattice diffusion, with emphasis on accessory minerals in crustal rocks. Am. Mineral. 80, 1179–1187.

Watson, E.B., Lupulescu, A., 1993. Aqueous fluid connectivity and chemical transport in clinopyroxene-rich rocks. Earth Planet. Sci. Lett. 117, 279–294.

White, W.B., Roy, R., 1964. Phase relations in the system lead–oxygen. J. Am. Ceram. Soc. 47, 242–249.

Wiedenbeck, M., Allé, P., Corfu, F., Griffin, W.L., Meier, M., Oberli, F., von Quadt, A., Roddick, J.C., Spiegel, W., 1995. Three natural zircon standards for U–Th–Pb, Lu–Hf, trace element and REE analyses. Geostand. Newslett. 19, 1–23.

Woodhead, J., Rossman, G.R., Thomas, A.P., 1991. Hydrous species in zircon. Am. Mineral. 76, 1533–1546.